

Published in final edited form as:

Acta Neuropathol. 2024 May 17; 147(1): 86. doi:10.1007/s00401-024-02741-x.

Tau filaments with the chronic traumatic encephalopathy fold in a case of vacuolar tauopathy with *VCP* mutation D395G

Chao Qi^{#1}, Ryota Kobayashi^{#2}, Shinobu Kawakatsu³, Fuyuki Kametani⁴, Sjors H.W. Scheres^{1,@}, Michel Goedert^{1,@}, Masato Hasegawa^{4,@}

¹Medical Research Council Laboratory of Molecular Biology, Cambridge, UK

²Department of Psychiatry, Yamagata University School of Medicine, Yamagata, Japan

³Department of Neuropsychiatry, Aizu Medical Center, Fukushima Medical University, Aizuwakamatsu, Japan

⁴Department of Brain and Neuroscience, Metropolitan Institute of Medical Science, Tokyo, Japan

These authors contributed equally to this work.

Abstract

Dominantly inherited mutation D395G in the gene encoding valosin-containing protein causes vacuolar tauopathy, a type of behavioural-variant frontotemporal dementia, with marked vacuolation and abundant filamentous tau inclusions made of all six brain isoforms. Here we report that tau inclusions were concentrated in layers II/III of the frontotemporal cortex in a case of vacuolar tauopathy. By electron cryo-microscopy, tau filaments had the chronic traumatic encephalopathy (CTE) fold. Tau inclusions of vacuolar tauopathy share this cortical location and the tau fold with CTE, subacute sclerosing panencephalitis and amyotrophic lateral sclerosis/parkinsonism-dementia complex, which are believed to be environmentally induced. Vacuolar tauopathy is the first inherited disease with the CTE tau fold.

Keywords

Valosin-containing protein; Mutation; Tauopathy; Neocortical layers II/III; Tau fold of chronic traumatic encephalopathy; Electron cryomicroscopy

This work is licensed under a [BY 4.0 International license](https://creativecommons.org/licenses/by/4.0/).

@To whom correspondence should be addressed: scheres@mrc-lmb.cam.ac.uk; mg@mrc-lmb.cam.ac.uk; hasegawa-ms@igakuken.or.jp .

Author contributions

RK and SK identified the patient and performed genetic analysis and neuropathology; MH prepared filaments and performed immunoblots; CQ performed cryo-EM data acquisition and structure determination; SHWS, MG and MH supervised the project and all authors contributed to the writing of the manuscript.

Conflict of interest The authors declare that they have no conflicts of interest.

Ethics approval and consent Studies carried out at Yamagata University were approved through the Institution's ethical review process. Informed consent was obtained from the patient's next of kin. This study was approved by the Cambridgeshire 2 Research Ethics Committee (09/H0308/163).

Introduction

Dominantly inherited mutation D395G in the gene encoding valosin-containing protein (*VCP*) has been described as the cause of an inherited form of behavioural-variant frontotemporal dementia (FTD) in three families from Greece, the US and Japan [5,20,35]. By histology and immunoblotting, abundant neuronal vacuoles and tau protein inclusions made of all six brain tau isoforms were in evidence in the Greek and US families, resulting in the naming of this condition as vacuolar tauopathy [5].

Previously, abundant tau inclusions were described in cases with mutations in genes other than *MAPT*, the tau gene. They include Alzheimer's disease (AD) (*APP* and presenilin genes), familial British and Danish dementias (*BRI* gene), and cases of Gerstmann-Sträussler-Scheinker disease (prion protein gene) [21]. In these diseases, abundant extracellular deposits of various proteins ($A\beta$, *BRI* and prion protein) are present alongside intraneuronal tau inclusions. By electron cryo-microscopy (cryo-EM), the Alzheimer tau fold is characteristic of these diseases [8,39].

The Alzheimer tau fold also characterises what has been called primary age-related tauopathy (PART) [43], a sporadic condition where tau inclusions form in an age-related manner, in the absence of extracellular deposits [3]. It follows that the tau inclusions that form in most people as a function of age have the Alzheimer fold.

Mutations in *MAPT* give rise to cases of frontotemporal dementia and parkinsonism linked to chromosome 17 (FTDP-17), with abundant tau inclusions in brain cells, in the absence of extracellular deposits [10]. So far, cryo-EM has shown the presence of Alzheimer [34], Pick [42] and argyrophilic grain disease [44] tau folds in cases of FTDP-17. Vacuolar tauopathy is the first disease caused by a mutation in a gene other than *MAPT* that results in the formation of abundant neuronal tau inclusions, in the absence of extracellular deposits.

By cryo-EM, tau filaments that are made of all six brain isoforms fall into two groups that consist of the Alzheimer and the chronic traumatic encephalopathy (CTE) folds [39]. The latter is also found in subacute sclerosing panencephalitis (SSPE) [32] and the amyotrophic lateral sclerosis/parkinsonism dementia complex (ALS/PDC) [33]. The CTE tau fold is typical of diseases with abundant inclusions in layers II/III of the neocortex. It consists mostly of repeats three and four, and 10-13 amino acids after repeat four (the longest human brain tau isoform of 441 amino acids has four microtubule-binding repeats of 31 or 32 amino acids each in its C-terminal half) [7].

Here we characterised the neuropathology and cryo-EM structures of tau filaments from a previously described individual with mutation D395G in *VCP* [20]. A Japanese man died aged 63 after an 18-year history of personality changes and cognitive impairment. Tau inclusions were present in the neocortex, where they were most abundant in layers II/III. Vacuolation was observed mostly in brain regions with few tau inclusions. By cryo-EM, the tau fold was identical to that in CTE, SSPE and ALS/PDC. This is the first inherited tauopathy with the CTE fold.

Materials and Methods

Clinical presentation

The individual was a man with a heterozygous D395G mutation in *VCP* who developed behavioural changes and cognitive impairment around age 45 [20]. He died of aspiration pneumonia aged 63. There was no history of head injury and the proband did not practice contact sports; he was not exposed to blast waves.

Immunohistochemistry

Neuropathological examination was carried out as described [17]. Briefly, one hemisphere was fixed in 10% neutral buffered formalin and cut into slices of 0.5 cm, whereas the other hemisphere was frozen. Tissue blocks were obtained from approximately thirty regions, including cerebral cortex, basal ganglia, brainstem and cerebellum. The tissues were embedded in paraffin and sectioned at 7 μm for Gallyas-Braak and 4 μm for haematoxylin-eosin (HE) staining and immunolabelling. For single-labelling immunohistochemistry, the following primary antibodies were used: AT8, to detect pS202/pT205 tau (1:1,000, Thermo Fisher Scientific), RD3, to detect 3R tau (1:250, Merck Millipore), anti-4R, to detect 4R tau deamidated at N279 (1:1,000, Cosmo Bio); anti-A β (11-28) (1:400, Immuno-Biological Laboratories); pSyn64, to detect α -synuclein phosphorylated at S129 (1:10,000, Fujifilm); pTDP-43, to detect TDP-43 phosphorylated at S409 and S410 (1:5,000, Cosmo Bio); anti-gial fibrillary acidic protein (1:400, Leica Biosystems); anti-Iba1 (1:1,000, Fujifilm). Primary antibody binding was detected using peroxidase-labelled streptavidin biotin kits (Nichirei histofine simole stain). Diaminobenzidine was used for colour development and the slides were counterstained with HE. Antigen retrieval used formic acid treatment [RD3, anti-4R and A β (11-28) antibodies] or autoclaving [pSyn64, pTDP-43 and glial fibrillary acidic protein antibodies]. Double-labelling immunofluorescence was performed essentially as described (45). Briefly, paraffin sections were deparaffinised and autoclaved for 20 min at 121° C in 10 mM Tris-buffer, pH 9.0, followed by a 5 min treatment with formic acid. After washing with water, the sections were treated with 3% hydrogen peroxide and blocked with 10% calf serum/phosphate-buffered saline (PBS). They were then incubated overnight at room temperature with anti-tau antibody AT8 (1:500, Thermo Fisher Scientific) and polyclonal anti-gial fibrillary acidic protein antibody (1:500, Abcam) or with anti-tau antibody pS396 (1:500, Millipore) and monoclonal glial fibrillary acidic protein antibody (1:500, Diagnostic BioSystems) in 10% calf serum/PBS. Following washing in PBS, the sections were incubated for 2 h at room temperature in Alexa Fluor 488 anti-mouse IgG (1:500) and Alexa Fluor 568 anti-rabbit IgG (1:500). After washing in PBS, they were treated with Sudan black for 10 min and coverslipped with an encapsulant containing DAPI. Images were obtained using an all-in-one microscope/digital camera (BZ-X710, Keyence).

Filament extraction

Sarkosyl-insoluble material was extracted from the frontal and temporal cortex of the brain of the individual with mutation D395G in *VCP*, as well as from the temporal cortex of a neuropathologically confirmed case of sporadic AD, essentially as described [46]. Briefly, tissues were homogenised with a Polytron in 40 vol (w/v) extraction buffer consisting of 10 mM Tris-HCl, pH 7.4, 0.8 M NaCl, 10% sucrose and 1 mM EGTA. Homogenates

were brought to 2% sarkosyl and incubated for 30 min at 37° C. Following a 10 min centrifugation at 27,000 g, the supernatants were spun at 257,000 g for 30 min. Pellets were resuspended in 2 ml extraction buffer containing 1% sarkosyl and centrifuged at 166,000 g for 20 min. The resulting pellets were resuspended in 20 µl buffer containing 20 mM Tris-HCl, pH 7.4, 100 mM NaCl and used for subsequent analysis.

Immunoblotting

Immunoblotting was carried out as described [46]. Samples were run on 5-20% gradient gels (Fuji Film). Proteins were then transferred to a polyvinylidene difluoride (PVDF) membrane and incubated with phosphorylation-dependent anti-tau mouse monoclonal antibody AT8 (1:1,000) overnight at room temperature. Following washing in PBS, the membranes were incubated with biotinylated anti-mouse antibody (Vector, 1:500) for 2h at room temperature, followed by a 30 min incubation with avidin-biotin complex and colour development using NiCl₂-enhanced diaminobenzidine.

Mass spectrometry

Sarkosyl-insoluble fractions from the frontal cortex of the individual with mutation D395G in *VCP* were treated with 70% formic acid for 1h at room temperature, diluted with water and dried. For trypsin digestion, 50 mM triethylammonium bicarbonate and 1 µg of Trypsin/Lys-C mix (Promega) were added. Each mixture was incubated at 37° C for 20 h. Following digestion, 2 µl of 100 mM dithiothreitol were added and the incubation continued at 100° C for 5 min. The samples were dried and stored at -80° C until use. Mass spectrometry was carried out as described [16].

Electron cryo-microscopy

Cryo-EM grids (Quantifoil 1.2/1.3, 300 mesh) were glow-discharged for 1 min using an Edwards (S150B) sputter coater. Three µl of the sarkosyl-insoluble fractions were applied to the glow-discharged grids, followed by blotting with filter paper and plunge freezing into liquid ethane using a Vitrobot Mark IV (Thermo Fisher Scientific) at 4° C and 100% humidity. Cryo-EM images were acquired on a Titan Krios G2 microscope (Thermo Fisher Scientific) operated at 300 kV and equipped with a Falcon-4i electron detector. Images were recorded for 2s in electron event representation format [11], with a total dose of 40 electrons per A² and a pixel size of 0.824 Å. See Supplementary Table 1 for further details.

Data processing

Datasets were processed in RELION using standard helical reconstruction [13,19]. Movie frames were gain-corrected, aligned and dose-weighted using RELION's own motion correction programme [50]. Contrast transfer function (CTF) was estimated using CTFFIND4.1 [36]. Filaments were picked by hand and segments were extracted with a box size of 1,024 pixels, prior to downsizing to 256 pixels. Reference-free 2D classification was carried out and selected class averages were re-extracted using a box size of 400 pixels. Initial models were generated *de novo* from 2D class average images using *reliion_helix_inimodel2d* [38]. Three-dimensional refinements were performed in RELION-4.0 and the helical twist and rise refined using local searches. Bayesian

polishing and CTF refinement were used to further improve resolutions [51]. The final maps were sharpened using standard post-processing procedures in RELION-4.0 and resolution estimates were calculated based on the Fourier shell correlation (FSC) between two independently refined half-maps at 0.143 (Supplementary Figure 1) [37]. We used `relion_helix_toolbox` to impose helical symmetry on the post-processed maps.

Model building and refinement

Atomic models were built manually using Coot [6], based on published structures (CTE Type I, PDB: 6NWP; CTE Type II, PDB: 6NWQ; CTE Type III, PDB: 8OT9) [7,33]. Model refinements were performed using ISOLDE [4], *Servalcat* [49] and REFMAC5 [26,27]. Models were validated with MolProbity [2]. Figures were prepared with ChimeraX [29] and PyMOL [41].

Results

At autopsy, the brain from the individual with mutation D395G in *VCP* weighed 968 g. A side view of the intact brain showed atrophy of the frontal cortex (Figure 1a). Coronal sections revealed moderate atrophy of the frontal cortex, with mild atrophy of temporal and parietal cortices, and no atrophy of occipital cortex, hippocampus, amygdala or basal ganglia (Figure 1b-d). There was depigmentation of the locus coeruleus, but not the substantia nigra.

Abundant tau-immunoreactive, Gallyas-Braak silver-positive neurofibrillary lesions, including ghost tangles, were observed in frontal (Figure 2a,d; Figure 3), temporal (Figure 2b,e; Figure 4) and parietal (Figure 2c,f) cortices. They were rare in occipital cortex and hippocampus (Figure 2b,c,e,f; Figure 5b,c,e,f,h,i). Neuronal cell loss (Figure 3a,h,o; Figure 4a,h,o) and neurofibrillary lesions were concentrated in the upper cortical layers of frontal (Figure 3b-e, i-l) and temporal (Figure 4b-e, i-l) cortices. They were also abundant in nucleus basalis of Meynert, thalamus, substantia nigra, caudate nucleus, locus coeruleus, pons and medulla oblongata. The cerebellum was well preserved, with only a few neurofibrillary lesions in the dentate nucleus. Double-labelling immunohistochemistry of frontal cortex sections for anti-tau antibody AT8 and glial fibrillary acidic antibody or for anti-tau antibody pS396 and glial fibrillary acidic protein showed no evidence of co-localisation (Supplementary Figure 2). There were no tau-immunoreactive cells in the depths of sulci.

As shown in Figure 3 (d,e,k,l) and Figure 4 (d,e,k,l), staining for 3R tau exceeded that for 4R tau in layers II/III; this correlated with the presence of ghost tangles, in agreement with a previous report [12]. The latter mainly consist of the ordered tau filament core (R3, R4 and 10-13 amino acids after R4). The presence of ghost tangles was also consistent with the stronger cell body staining for Gallyas-Braak silver than for tau phosphorylated at pS202/pT205 (antibody AT8) (Figures 3b,c,i,j; 4b,c,i,j). Strong neuritic staining by AT8 (Figures 3c,j; 4c,j) may have been the result of afferent projections with tau inclusions.

Severe vacuolar changes were observed predominantly in the superficial layers of the primary visual cortex (Figure 5a,d), where neurofibrillary lesions (Figure 5b,c,e,f,h,i) were almost absent. Mild vacuolar changes were also present in frontal (Figure 3o) and temporal

(Figure 4h) cortices. Astrogliosis and activation of microglia were evident in frontal (Figure 3f,g,m,n,t,u) and temporal (Figure 4f,g,m,n,t,u) cortices. This case is thus another example of vacuolar tauopathy caused by mutation D395G in *VCP*.

Immunoblotting of the sarkosyl-insoluble fraction from the temporal cortex of the individual with vacuolar tauopathy with anti-tau antibody AT8 showed the presence of strong bands of 60, 64 and 68 kDa and a weak band of 72 kDa. This pattern was identical to that from a case of sporadic AD (Figure 6). The post-translational modifications of sarkosyl-insoluble tau extracted from the frontal cortex of the individual with vacuolar tauopathy (Supplementary Table 2) were also similar to those reported in AD [16,48]. No A β , α -synuclein or TDP-43 inclusions were observed.

We used cryo-EM to determine the structures of tau filaments extracted from the frontal and temporal cortices of the individual with vacuolar tauopathy. Three types of filaments were observed that were made of two identical protofilaments arranged in different ways (Figure 7a,b). All three filament types were found in the frontal cortex, with Type III being absent from the temporal cortex. Filament structures were determined to resolutions ranging from 2.3 to 3.4 Å, which allowed us to establish their identity as CTE filament Types I-III [7,32] (Figure 7c). The ordered cores of the filaments span residues K274-R379 of three-repeat tau and S305-R379 of four-repeat tau.

Discussion

Mutation D395G in *VCP* causes vacuolar tauopathy, a type of frontotemporal dementia with widely distributed and abundant filamentous tau inclusions [5]. Here we report the neuropathology from a previously described case with mutation D395G in *VCP* [20] and establish that it is a case of vacuolar tauopathy.

In the neocortex, Gallyas-Braak silver-positive tau inclusions were concentrated in the superficial layers. Inclusions were present in frontal, temporal and parietal cortices, as well as in several other brain regions. The frontal cortex was moderately atrophic. Immunoblotting showed a pattern of tau bands like that in AD and CTE, consistent with the presence of all six brain tau isoforms [9,40]. By mass spectrometry, the post-translational modifications of sarkosyl-insoluble tau extracted from the frontal cortex of the individual with vacuolar tauopathy were like those in AD [16,48].

Neuronal vacuolation and neurofibrillary degeneration were inversely related. Thus, abundant vacuoles were found mostly in regions that had only few neurofibrillary lesions, such as the occipital cortex. Conversely, regions with abundant tau inclusions, such as the frontal and temporal cortices, had only few vacuoles. This suggests that the D395G mutation in *VCP* causes neuronal vacuolation and neurofibrillary degeneration through distinct mechanisms. Astrocytosis and microgliosis were seen in regions with neurofibrillary degeneration, as is the case of other diseases with neurofibrillary tau pathology [18].

These findings are reminiscent of those reported previously in four individuals from two families with mutation D395G in *VCP* [5]. Vacuolation appeared to be endocytic and was found mostly in cells that were not destined for neurodegeneration. The previous work

also hypothesised that VCP might be a disaggregase for assembled and ubiquitinated tau, with assembled tau accumulating as the result of a partial loss-of-function resulting from mutation D395G. However, it was surprising that this mutation did not appear to affect other proteins known to aggregate in a polyubiquitinated form in the human brain, such as α -synuclein and TDP-43. *In vitro* experiments have shown that VCP prevents the seeding, not only of assembled tau [5], but also of assembled α -synuclein and TDP-43 [52].

VCP is an AAA⁺ ATPase that unfolds ubiquitinated proteins [1]. Besides mutation D395G, other mutations in *VCP* cause multisystem proteinopathy, a degenerative disease affecting muscle and bone, that can also present as frontotemporal dementia with TDP-43 inclusions [30,46]. Unlike D395G, which results in a reduction in the ATPase activity of VCP [5], these mutations increase the ATPase activity and are believed to result in a gain-of-toxic function of VCP.

We used cryo-EM to determine the fold of tau filaments extracted from the frontal and temporal cortices of the individual with vacuolar tauopathy. The filaments had the CTE tau fold [7], which we also identified in cases of SSPE [32] and ALS-PDC [33]. Types I-III of CTE filaments [7,32] were present in the frontal cortex, with only Types I and II being found in the temporal cortex. The three types of filaments are molecular polymorphs consisting of two identical protofilaments that are linked in different ways. In these diseases, more filamentous tau inclusions are found in layers II/III of the cerebral cortex than in layer V [14,24,25]. This is unlike AD, where tau inclusions are more abundant in layer V [28].

So far, there has been an absolute correlation between the cortical localisation of tau inclusions and the presence of the CTE or the Alzheimer fold. Even though the relevant tau folds are not known, it is tempting to speculate that the CTE fold may also form in other diseases with a predominance of tau inclusions in cortical layers II/III, such as postencephalitic parkinsonism [15] and the nodding syndrome [31]. However, unlike CTE, SSPE and ALS/PDC, which are believed to have mainly environmental causes, vacuolar tauopathy is dominantly inherited. It is the first inherited condition with the CTE tau fold. It remains to be determined if tau filaments extracted from the brains of other cases with vacuolar tauopathy [5] also carry the CTE fold.

The CTE tau fold differs from the Alzheimer fold by having a more open conformation of the β -helix region, which contains an internal density of unknown identity [7]. In the presence of NaCl, recombinant tau comprising residues 297-391 assembles into filaments with the CTE fold, but in the presence of MgCl₂, the Alzheimer fold forms [22]. Both folds assemble from a shared transient first intermediate amyloid filament, followed by multiple different polymorphic filamentous intermediates [23].

It remains to be determined how mutation D395G in *VCP* leads to the presence of tau filaments with the CTE fold. VCP may be a disaggregase of this fold. On the other hand, we have previously hypothesised that the CTE tau fold could form in response to separate insults, which might be linked by specific neuroinflammatory changes that differ from those common to all tauopathies [33]. A partial loss-of-function of VCP could therefore give

rise to mechanisms that result in the formation of the CTE fold without requiring a direct interaction with tau.

Supplementary Material

Refer to Web version on PubMed Central for supplementary material.

Acknowledgements

This work was supported by the Electron Microscopy Facility of the MRC Laboratory of Molecular Biology. We thank Jake Grimmer, Toby Darling and Ivan Clayson for help with high-performance computing, and Takumi Kitaoka and Mitsuru Futakuchi (Yamagata University School of Medicine) for help with neuropathology. We also thank Hiroya Naruse and Tatsushi Toda (University of Tokyo) for genomic analysis. For open access, the MRC Laboratory of Molecular Biology has applied a CC BY public copyright licence to any Author Accepted Manuscript version arising.

Funding

This work was supported by the UK Medical Research Council (MC_UP_A025-1013 to S.H.W.S. and MC_U105184291 to M.G.), the Japanese Society for the Promotion of Science (JSPS KAKENHI and JP20K07922, to R.K. and S.K.) and the Japanese Ministry of Health, Labour and Welfare (JPMH20GB1002 and JPMH23GB1003, to R.K. and S.K.).

References

1. Bodnar NO, Rapoport TA. Molecular mechanism of substrate processing by the Cdc48 ATPase complex. *Cell*. 2017; 169: 722–725. [PubMed: 28475898]
2. Chen VB, Arendall WB, Headd JJ, Keedy DA, Immormino RM, Kaprai GI, et al. MolProbity: All-atom structure validation for macromolecular crystallography. *Acta Crystallogr D*. 2010; 66: 12–21. [PubMed: 20057044]
3. Crary JF, Trojanowski JQ, Schneider JA, Abisambra JF, Abner EL, Alafuzoff I, et al. Primary age-related tauopathy (PART): A common pathology associated with human aging. *Acta Neuropathol*. 2014; 128: 755–766. [PubMed: 25348064]
4. Croll TI. ISOLDE: A physically realistic environment for model building into low-resolution electron density map. *Acta Crystallogr D*. 2018; 74: 519–530.
5. Darwich NF, Phan JM, Kim E, Suh ER, Papatriantafyllou JD, Changolkar L, et al. Autosomal dominant VCP hypomorph mutation impairs disaggregation of PHF-tau. *Science*. 2020; 370 eaay8826 [PubMed: 33004675]
6. Emsley P, Lohkamp B, Scott WG, Cowtan K. Features and development of Coot. *Acta Crystallogr D*. 2010; 66: 486–501. [PubMed: 20383002]
7. Falcon B, Zivanov J, Zhang W, Murzin AG, Garringer HJ, Vidal R, et al. Novel tau filament fold in chronic traumatic encephalopathy encloses hydrophobic molecules. *Nature*. 2019; 568: 420–423. [PubMed: 30894745]
8. Fitzpatrick AWP, Falcon B, He S, Murzin AG, Murshudov G, Garringer HJ, et al. Cryo-EM structures of tau filaments from Alzheimer's disease. *Nature*. 2017; 547: 185–190. [PubMed: 28678775]
9. Goedert M, Spillantini MG, Cairns NJ, Crowther RA. Tau proteins of Alzheimer paired helical filaments: Abnormal phosphorylation of all six brain isoforms. *Neuron*. 1992; 8: 159–168. [PubMed: 1530909]
10. Goedert M, Crowther RA, Scheres SHW, Spillantini MG. Tau and neurodegeneration. *Cytoskeleton*. 2024; 81: 95–102. [PubMed: 38073060]
11. Guo H, Franken E, Deng Y, Benlekbir S, Lezcano GS, Janssen B, et al. Electron-event representation data enable efficient cryo-EM file storage with full preservation of spatial and temporal resolution. *IUCrJ*. 2020; 7: 860–869.

12. Hasegawa M, Watanabe S, Kondo H, Akiyama H, Mann DMA, Saito Y, et al. 3R and 4R tau isoforms in paired helical filaments in Alzheimer's disease. *Acta Neuropathol.* 2014; 127: 303–305. [PubMed: 24212601]
13. He S, Scheres SHW. Helical reconstruction in RELION. *J Struct Biol.* 2017; 193: 163–176.
14. Hof PR, Bouras C, Buée L, Delacourte A, Perl DP, Morrison JH. Differential distribution of neurofibrillary tangles in the cerebral cortex of dementia pugilistica and Alzheimer's disease cases. *Acta Neuropathol.* 1992; 85: 23–30. [PubMed: 1285493]
15. Hof PR, Charpiot A, Delacourte A, Buée L, Purohit D, Perl DP, et al. Distribution of neurofibrillary tangles and senile plaques in the cerebral cortex in postencephalitic parkinsonism. *Neurosci Lett.* 1992; 139: 10–14. [PubMed: 1407674]
16. Kametani F, Yoshida M, Matsubara T, Murayama S, Saito Y, Kawakami I, et al. Comparison of common and disease-specific post-translational modifications of pathological tau associated with a wide range of tauopathies. *Front Neurosci.* 2020; 14 581936 [PubMed: 33250706]
17. Kawakatsu S, Kobayashi R, Hayashi H, Morioka D, Utsunomiya A, Kabasawa T, et al. Clinicopathological heterogeneity of Alzheimer's disease with pure Alzheimer's disease pathology: Cases associated with dementia with Lewy bodies, very early-onset dementia, and primary progressive aphasia. *Neuropathology.* 2021; 41: 427–449. [PubMed: 34816507]
18. Keren-Shaul H, Spinrad A, Weinmer A, Matcovitch-Natan O, Dvir-Szrenfeld R, Ulland TK, et al. A unique microglia type associated with restricting development of Alzheimer's disease. *Cell.* 2017; 169: 1276–1290. [PubMed: 28602351]
19. Kimanius D, Dong L, Sharov G, Nakane T, Scheres SHW. New tools for automated cryo-EM single-particle analysis in RELION-4.0. *Biochem J.* 2021; 478: 4169–4185. [PubMed: 34783343]
20. Kobayashi R, Naruse H, Kawakatsu S, Iseki C, Suzuki Y, Koyama S, et al. Valosin-containing protein Asp395Gly mutation in a patient with frontotemporal dementia: a case report. *BMC Neurol.* 2022; 22: 406. [PubMed: 36329418]
21. Kovacs GG, Ghetti B, Goedert M. Classification of diseases with accumulation of tau protein. *Neuropathol Appl Neurobiol.* 2022; 48 e12792 [PubMed: 35064600]
22. Lövestam S, Koh FA, van Knippenberg B, Kotecha A, Murzin AG, Goedert M, et al. Assembly of recombinant tau into filaments identical to those of Alzheimer's disease and chronic traumatic encephalopathy. *eLife.* 2022; 11 e76494 [PubMed: 35244536]
23. Lövestam S, Li D, Wagstaff JL, Kotecha A, Kimanius D, McLaughlin SH, et al. Disease-specific tau filaments assemble via polymorphic intermediates. *Nature.* 2024; 625: 119–125. [PubMed: 38030728]
24. Mimuro M, Yoshida S, Kuzuhara S, Kokubo Y. Amyotrophic lateral sclerosis and parkinsonism-dementia complex of the Hohara focus of the Kii peninsula: A multiple proteinopathy? *Neuropathology.* 2018; 38: 98–107. [PubMed: 29063640]
25. Miyahara H, Akagi A, Riku Y, Sone J, Otsuka Y, Sakai M, et al. Independent distribution between tauopathy secondary to subacute sclerosing panencephalitis and measles virus. *Brain Pathol.* 2022; 32 e13069 [PubMed: 35373453]
26. Murshudov GN, Vagin AA, Dodson EJ. Refinement of macromolecular structures by the maximum-likelihood method. *Acta Crystallogr D.* 1997; 53: 240–255. [PubMed: 15299926]
27. Murshudov GN, Skubák P, Lebedev AA, Pannu NS, Steiner RA, Nicholls RA, et al. REFMAC5 for the refinement of macromolecular crystal structures. *Acta Crystallogr D.* 2011; 67: 255–267.
28. Pearson RCA, Esiri MM, Hiorns RW, Wilcock GK, Powell TPS. Anatomical correlates of the distribution of the pathological changes in the neocortex in Alzheimer disease. *Proc Natl Acad Sci USA.* 1985; 82: 4531–4534. [PubMed: 3859874]
29. Pettersen EF, Goddard TD, Huang CC, Meng EC, Couch GS, Croll TI, et al. Chimera X: Structure visualization for researchers, editors and developers. *Protein Sci.* 2011; 30: 70–82.
30. Pfeffer G, Lee G, Pontifex CS, Fanganiello RD, Peck A, Weihl CC, et al. Multisystem proteinopathy due to VCP mutations: A review of clinical heterogeneity and genetic diagnosis. *Genes.* 2022; 13: 963. [PubMed: 35741724]
31. Pollanen MS, Onzivua S, McKeever PM, Robertson J, Mackenzie IR, Kovacs GG, et al. The spectrum of disease and tau pathology of nodding syndrome in Uganda. *Brain.* 2023; 146: 954–967. [PubMed: 35411378]

32. Qi C, Hasegawa M, Takao M, Sakai M, Sasaki M, Mizutani M, et al. Identical tau filaments in subacute sclerosing panencephalitis and chronic traumatic encephalopathy. *Acta Neuropathol Commun.* 2023; 11: 74. [PubMed: 37143123]
33. Qi C, Verheijen BM, Kokubo Y, Shi Y, Tetter S, Murzin AG, et al. Tau filaments from amyotrophic lateral sclerosis/parkinsonism-dementia complex adopt the CTE fold. *Proc Natl Acad Sci USA.* 2023; 120 e2306767120 [PubMed: 38100415]
34. Qi C, Lövestam S, Murzin AG, Peak-Chew S, Franco C, Bogdani M, et al. Tau filaments with the Alzheimer fold in cases with MAPT mutations V337M and R406W. *BioRxiv.* 2024.
35. Ramos AM, Koros C, Dokuru DR, Van Berlo V, Kroupis C, Wojta K, et al. Frontotemporal dementia spectrum: first genetic screen in a Greek cohort. *Neurobiol Aging.* 2019; 224: e1–e8.
36. Rohou A, Grigorieff N. CTFFIND4: Fast and accurate defocus estimation from electron micrographs. *J Struct Biol.* 2015; 192: 216–221. [PubMed: 26278980]
37. Scheres SHW, Chen S. Prevention of overfitting in cryo-EM structure determination. *Nature Meth.* 2012; 9: 8453–8454.
38. Scheres SHW. Amyloid structure determination in RELION-3.1. *Acta Cryst D.* 2020; 76: 94–101.
39. Scheres SHW, Ryskeldi-Falcon B, Goedert M. Molecular pathology of neurodegenerative diseases by cryo-EM of amyloids. *Nature.* 2023; 621: 701–710. [PubMed: 37758888]
40. Schmidt ML, Zhukareva V, Newell KL, Lee VMY, Trojanowski JQ. Tau isoform profile and phosphorylation state in dementia pugilistica recapitulate Alzheimer’s disease. *Acta Neuropathol.* 2001; 101: 5128–524.
41. Schrödinger L, DeLano W. PyMol. 2020. available at : <http://www.pymol.org/pymol>
42. Schweighauser M, Garringer HJ, Klingstedt T, Nilsson KPR, Masami-Suzukake M, Murrell JR, et al. Mutation K281 in *MAPT* causes Pick’s disease. *Acta Neuropathol.* 2023; 146: 211–226. [PubMed: 37351604]
43. Shi Y, Murzin AG, Falcon B, Epstein A, Machin J, Tempest P, et al. Cryo-EM structures of tau filaments from Alzheimer’s disease with PET ligand APN-1607. *Acta Neuropathol.* 2021; 141: 697–708. [PubMed: 33723967]
44. Shi Y, Zhang W, Yang Y, Murzin AG, Falcon B, Kotecha A, et al. Structure-based classification of tauopathies. *Nature.* 2021; 598: 359–363. [PubMed: 34588692]
45. Shimozawa A, Ono M, Takahara D, Tarutani A, Imura S, Masuda-Suzukake M, et al. Propagation of pathological α -synuclein in marmoset brain. *Acta Neuropathol Commun.* 2017; 5: 12. [PubMed: 28148299]
46. Tarutani A, Arai T, Murayama S, Hisanaga SI, Hasegawa M. Potent prion-like behaviors of pathogenic α -synuclein and evaluation of inactivation methods. *Acta Neuropathol Commun.* 2018; 6: 29. [PubMed: 29669601]
47. Watts GD, Wymer J, Kovach MJ, Mehta SG, Mumm S, Darvish D, et al. Inclusion body myopathy associated with Paget disease of bone and frontotemporal dementia is caused by mutant valosin-containing protein. *Nature Genet.* 2004; 36: 377–381. [PubMed: 15034582]
48. Wesseling H, Mair W, Kumar M, Schläffner CN, Tang S, Beerepoot O, et al. Tau PTM profiles identify patient heterogeneity and stages of Alzheimer’s disease. *Cell.* 2020; 183: 1699–1713. [PubMed: 33188775]
49. Yamashita K, Palmer CM, Burnley T, Murshudov GN. Cryo-EM single particle structure refinement and map calculation using Servalcat. *Acta Crystallogr D.* 2021; 77: 1282–1291.
50. Zivanov J, Nakane T, Forsberg BO, Kimanius D, Hagen WJ, Lindahl E, et al. New tools for automated high-resolution cryo-EM structure determination in RELION-3. *eLife.* 2018; 7 e42166 [PubMed: 30412051]
51. Zivanov J, Otón J, Ke Z, von Kügelen E, Pyle E, Qu K, et al. A Bayesian approach to single-particle electron-tomography in RELION-4.0. *eLife.* 2022; 11 e83724 [PubMed: 36468689]
52. Zhu J, Pittman S, Dhavale D, French R, Patterson JN, Kaleelurrahuman MS, et al. VCP suppresses proteopathic seeding in neurons. *Mol Neurodegen.* 2022; 17: 30.

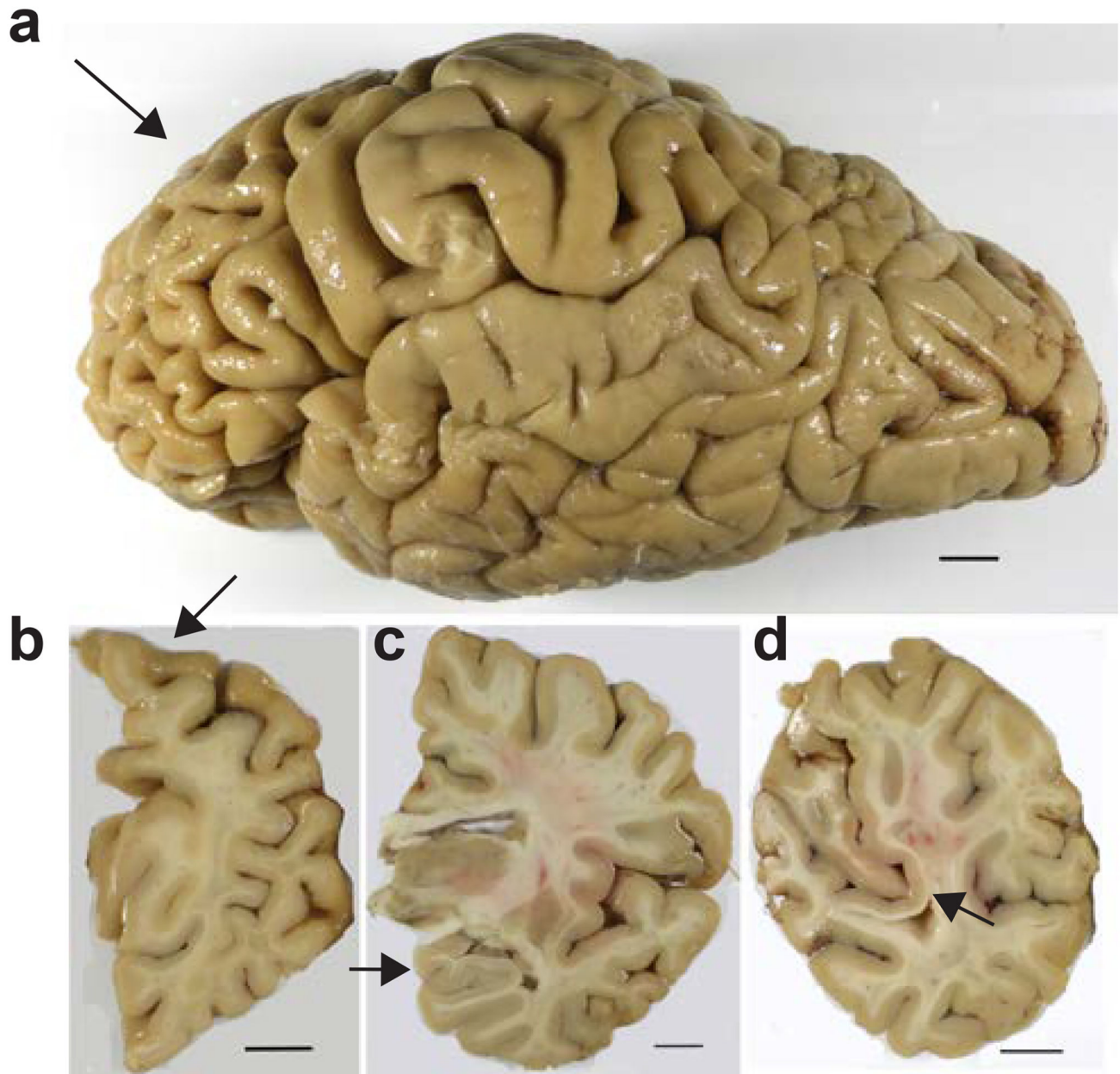


Figure 1. Formalin-fixed brain from the individual with mutation D395G in VCP.

a, Side view of the brain, showing atrophy of the frontal cortex (arrowed). b, Coronal section of the cerebral hemispheres with atrophy of the dorsal portion of the frontal lobe (arrowed).

c, Coronal section at the level of the thalamus, indicating preservation of the hippocampus (arrowed).

d, Coronal section showing preservation of the occipital cortex, including the primary visual cortex (arrowed).

Scale bars, 10 mm.

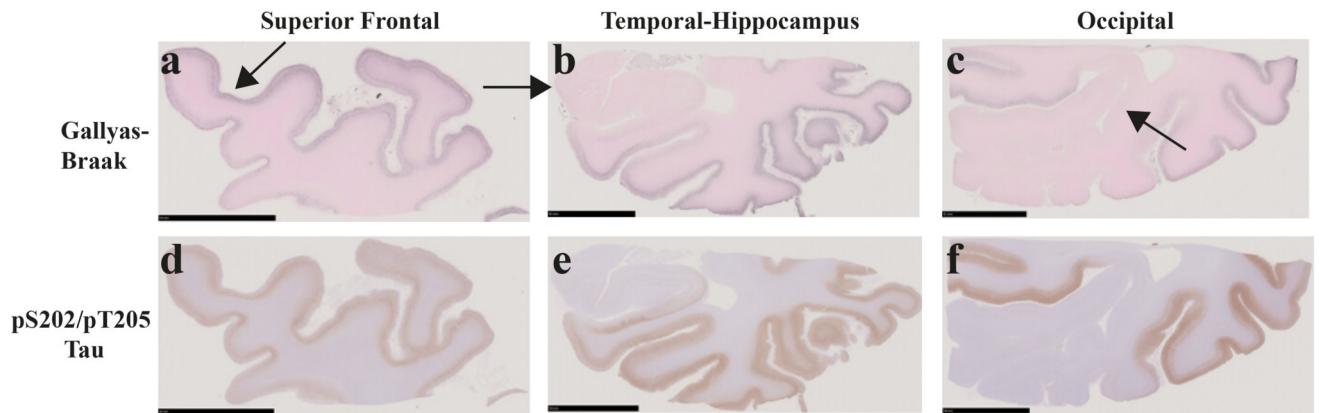


Figure 2. Gallyas-Braak silver and pTau (AT8) staining of coronal brain sections of the superior frontal, the temporal-hippocampus and the occipital cortex from the individual with mutation D395G in VCP.

a-c, Gallyas-Braak silver shows numerous lesions in the superficial layers of the atrophic superior frontal cortex (arrowed) (d), inferior to middle temporal (e) and occipital (f) cortex, whereas hippocampus (arrowed) and primary visual cortex (arrowed) are intact. Scale bars, 10 mm.

d-f, Similar to Gallyas-Braak silver, AT8 immunostaining shows strong staining of frontal, temporal and parietal cortical layers, with sparing of the hippocampus and the primary visual cortex. Scale bars, 10 mm.

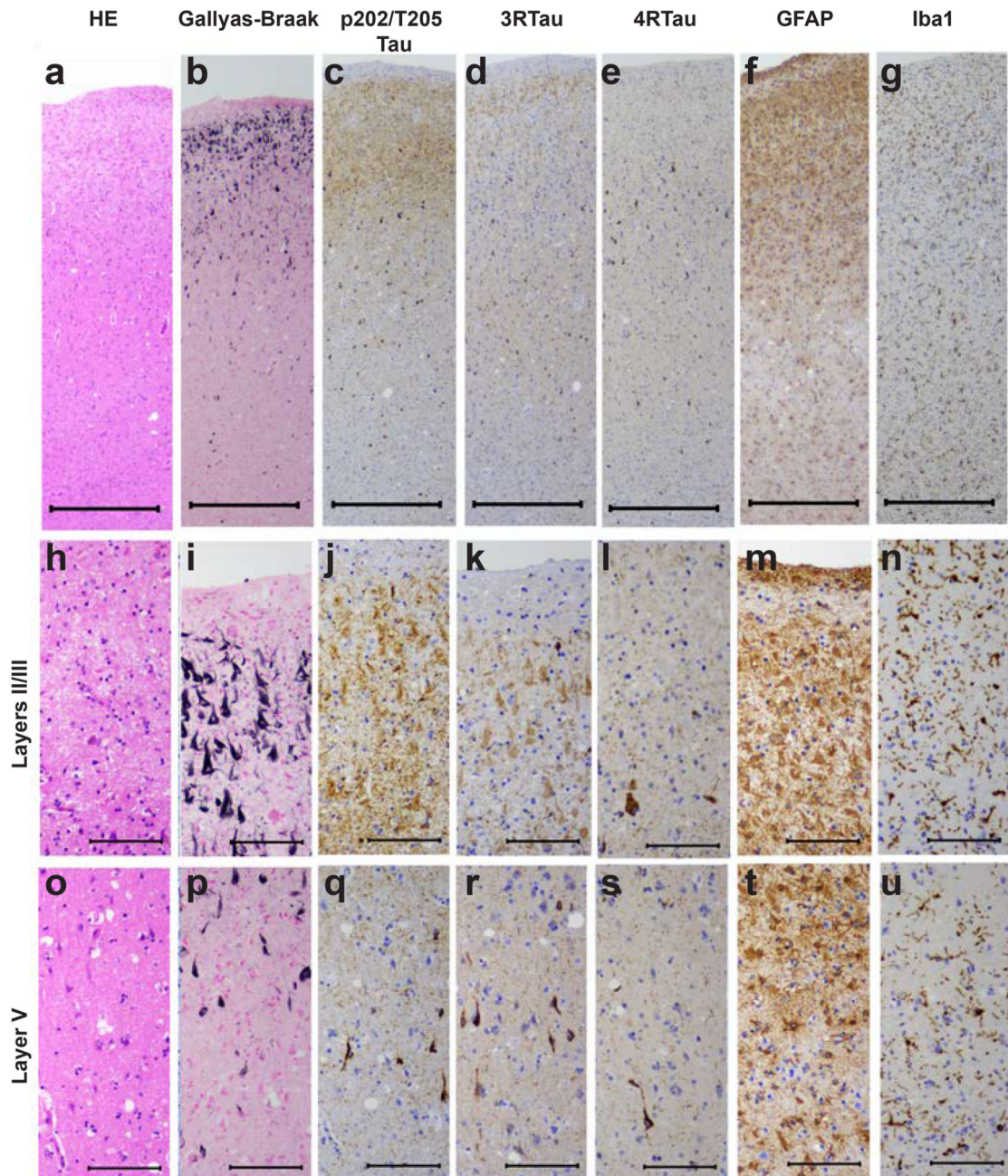


Figure 3. Staining of the superior frontal cortex in vacuolar tauopathy.

Nerve cell loss and gliosis are seen in layers II/III (a,f,g,h,m,n), where abundant tau-immunoreactive neurofibrillary lesions are in evidence (b,c,d,e,i,j,k,l). Fewer neurofibrillary lesions are seen in layer V (p,q,r,s). Mild vacuolar changes are present in layer V (o). Astroglia and microglial changes are most severe in the superficial cortical layers (f,g,m,n). HE staining (a,h,o); Gallyas-Braak silver (b,i,p); pTau (AT8) (c,j,q); 3R Tau (RD3) (d,k,r); 4R Tau (anti-4R) (e,l,s); GFAP (f,m,t); Iba1 (g,n,u). Scale bars: 500 μm (a-g), 100 μm (h-u).

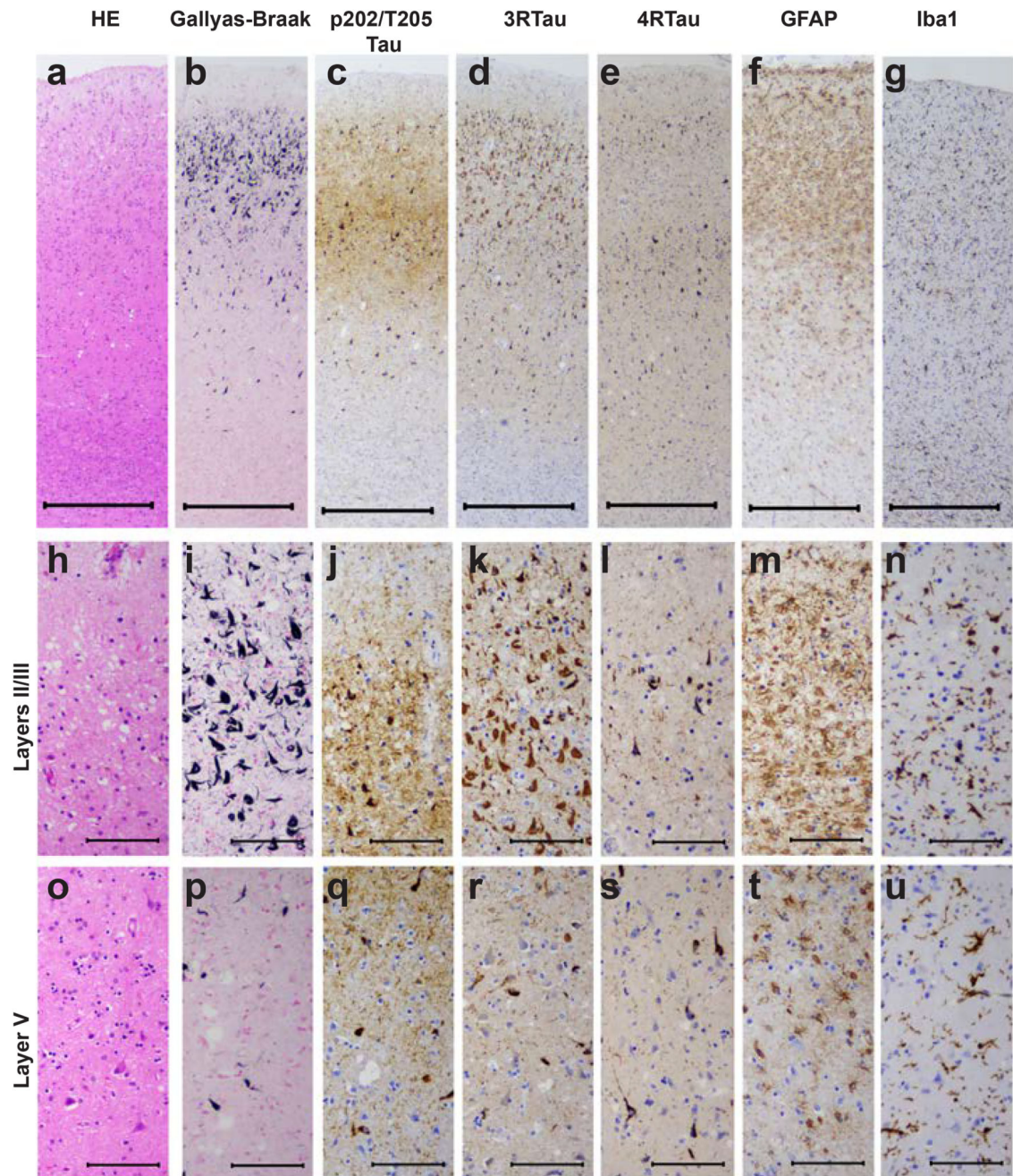


Figure 4. Staining of the middle temporal cortex in vacuolar tauopathy.

Nerve cell loss and gliosis are seen in layers II/III (a,f,g,h,m,n), where abundant tau-immunoreactive neurofibrillary lesions are in evidence (b,c,d,e,i,j,k,l). Fewer neurofibrillary lesions are seen in layer V (p,q,r,s). Mild vacuolar changes are present in layers II/III (h). Astroglia and microglial changes are most severe in the superficial cortical layers (f,g,m,n). HE staining (a,h,o); Gallyas-Braak silver (b,i,p); pTau (AT8) (c,j,g); eR Tau (RD3) (d,k,r); 4R Tau (anti-4R) (e,l,s); GFAP (f,m,t); Iba1 (g,n,u). Scale bars: 500 μ m (a-g), 100 μ m (h-u).

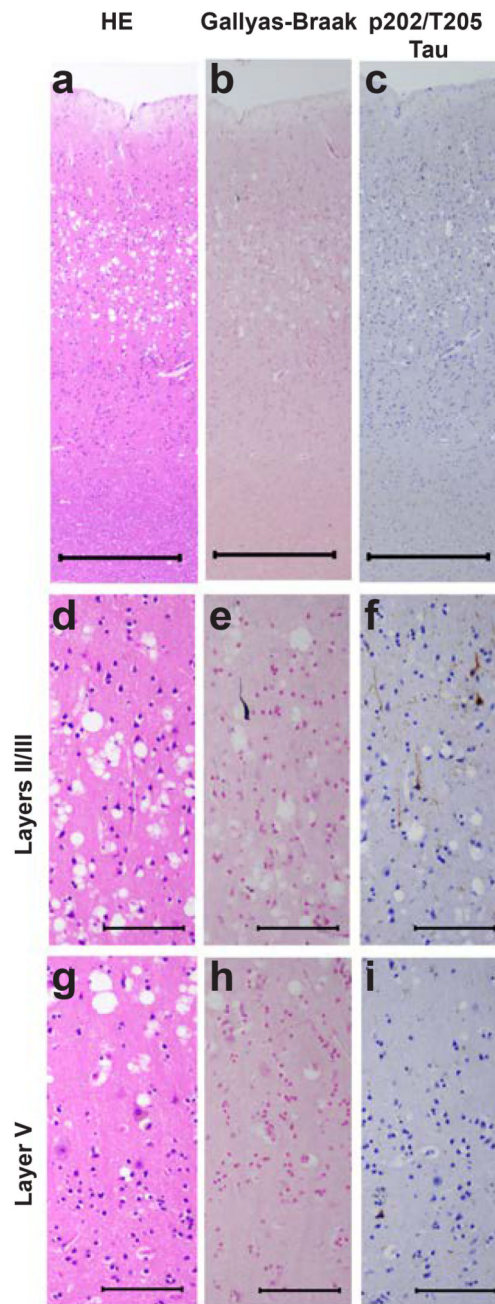


Figure 5. Staining of the primary visual cortex in vacuolar tauopathy. Neurofibrillary lesions are almost absent (b,c,e,f,h,i). Severe vacuolar changes are present, in particular in the superficial cortical layers (a,d,g). HE staining (a,d,g); Gallyas-Braak silver (b,e,h); pTau (AT8) (c,f,i). Scale bars: 500 μ m (a-c), 100 μ m (d-i).

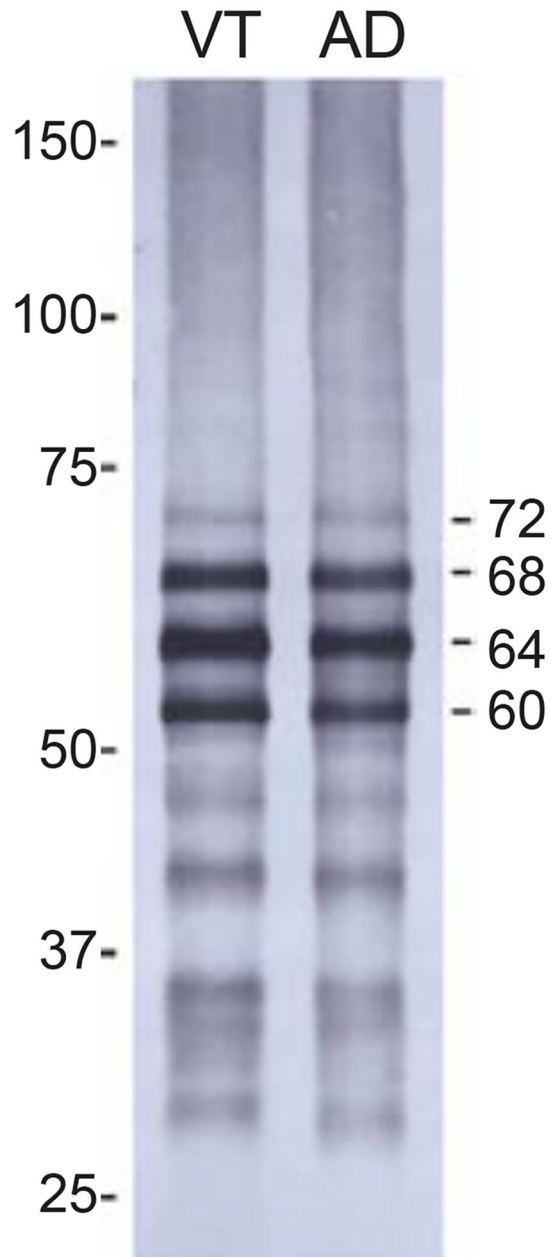


Figure 6. Immunoblotting of sarkosyl-insoluble fractions from the temporal cortex of the individual with vacuolar tauopathy (VT) and a case of sporadic Alzheimer's disease (AD). Phosphorylation-dependent anti-tau antibody AT8 was used. Note the presence of strong bands of 60, 64 and 68 kDa and a weaker band of 72 kDa (indicated on the right).

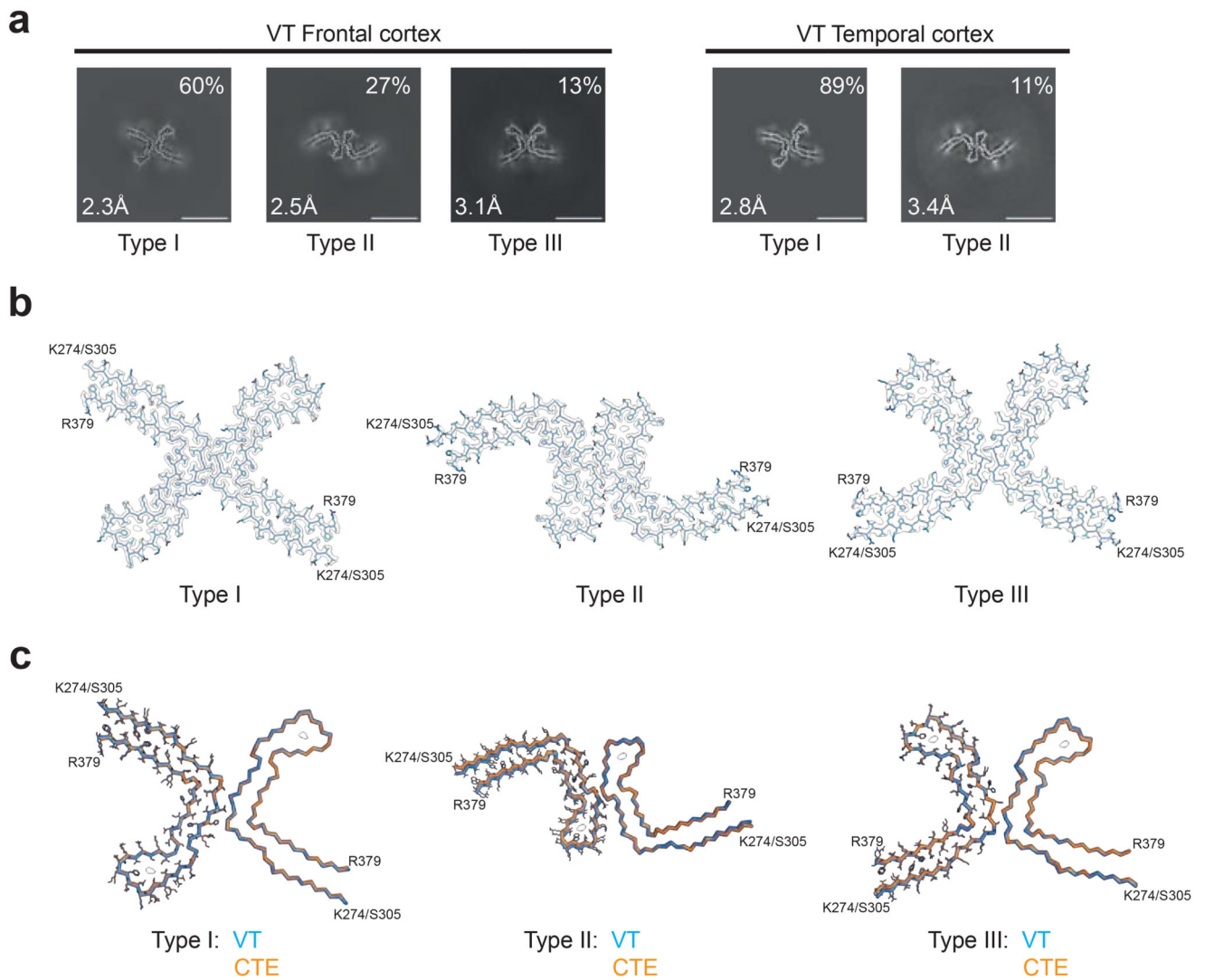


Figure 7. Cryo-EM cross-sections and structures of tau filaments from vacuolar tauopathy.
 a, Cross-sections through the cryo-EM reconstructions, perpendicular to the helical axis and with a projected thickness of approximately one rung, are shown for frontal and temporal cortex. Three filament types were present (Type III was only found in the frontal cortex). They are made of two identical protofilaments that are arranged in different ways. Resolutions (in Å) and percentages of filament types are indicated in the bottom left and top right, respectively. Scale bar, 10 nm.
 b, Cryo-EM density maps and models of Type I, Type II and Type III tau filaments from the case with vacuolar tauopathy.
 c, Type I, Type II and Type III filaments from the case with vacuolar tauopathy (in blue) overlaid with CTE Type I, Type II and Type III filaments from a case with CTE (in orange). The ordered cores of the filaments extend from tau K274/S305-R379.

The root mean square deviation (rmsd) between Ca atoms of Type I and CTE Type I filaments was 0.28 Å; that between Type II and CTE Type II filaments was 0.57 Å and that between Type III and CTE Type III filaments was 0.57 Å.